THE JOURNAL OF PHYSICAL CHEMISTRY B

Article

pubs.acs.org/JPCB

X-ray Free Electron Laser Radiation Damage through the S-State Cycle of the Oxygen-Evolving Complex of Photosystem II

Muhamed Amin,*[,†,‡] Mikhail Askerka,[§] Victor S. Batista,[§] Gary W. Brudvig,[§] and M. R. Gunner[∥]

[†]Center for Photonics and Smart Materials, Zewail City of Science and Technology, Sheikh Zayed District, 6th of October City, 12588 Giza, Egypt

[‡]Center for Free-Electron Laser Science, Deutsches Elektronen-Synchrotron DESY, Notkestrasse 85, 22607 Hamburg, Germany

[§]Department of Chemistry, Yale University, New Haven, Connecticut 06520-8107, United States

[∥]Department of Physics, City College of New York, New York, New York 10031, United States

Supporting Information

ABSTRACT: The oxygen-evolving complex (OEC) catalyzes water-splitting through a reaction mechanism that cycles the OEC through the "S-state" intermediates. Understanding structure/function relationsships of the S-states is crucial for elucidating the water-oxidation mechanism. Serial femtosecond X-ray crystallography has been used to obtain radiation damage-free structures. However, it remains to be established whether "diffraction-before-destruction" is actually accomplished or if significant changes are produced by the high-intensity X-ray pulses during the femtosecond scattering measurement. Here, we use *ab initio* molecular dynamics simulations to estimate the extent of structural changes induced on the femtosecond time scale. We found that the radiation damage is dependent on the bonding and charge of each atom in the OEC, in a manner that may provide lessons for XFEL studies of other metalloproteins. The maximum displacement of Mn and oxygen centers is 0.25 and 0.39 Å, respectively, during the 50 fs pulse, which is significantly smaller than the uncertainty given the 1.9 Å resolution of the current PSII crystal structures. However, these structural changes might be detectable when comparing isomorphous Fourier differences of electron density maps of the different S-states. One conclusion is that pulses shorter than 15 fs should be used to avoid significant radiation damage.

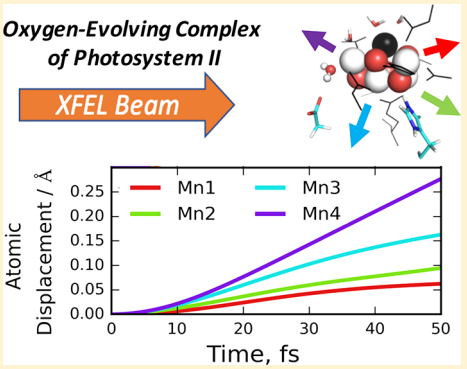

INTRODUCTION

Photosystem II (PSII) catalyzes O_2 evolution by water splitting at the oxygen-evolving complex (OEC), embedded in the D1 protein subunit.[1,2] The OEC is an oxomaganese core composed of four Mn ions and one Ca^{2+}, connected by oxo-bridges and coordinated by terminal water ligands and side-chains of surrounding amino-acid residues.[3] A complex chemical process cycles the OEC through five redox states (S_0, S_1, S_2, S_3, and the transient S_4), as it is oxidized four times in a sequence of catalytic steps before triggering the O−O bond formation leading to O_2 evolution. The transitions between S-states involve oxidation of Mn centers, upon visible light absorption by chlorophyll chromophores, leading to energy transfer, charge separation, and oxidation of the redox active tyrosine Z next to the OEC. All of the S-state transitions, except for $S_1 \rightarrow S_2$, involve deprotonation of the OEC to balance the positive charge left behind upon Mn oxidation. Because there is no proton release in the $S_1 \rightarrow S_2$ transition, a positive charge is accumulated at the Mn_4O_5Ca cluster.[4,5] Except for the O_2-evolving $S_4 \rightarrow S_0$ transition, the S-state transitions are all light-driven and take place in hundreds of microseconds.[6]

The structure of the OEC has been determined by conventional X-ray crystallography at 1.90 Å resolution, which is sufficient to begin to see the detailed structure of the Mn_4O_5Ca cluster.[3] However, the exposure to X-ray radiation during conventional X-ray crystallographic data collection likely induces reduction of the high-valent Mn ions, forming low-valent states, including Mn^{2+}, that do not correspond to any of the active S-state intermediates. Thus, although the 1.9 Å structure provided valuable structural information on the OEC, the data likely represent a mixture of states, including redox states of the OEC more reduced than S_0.[7,8] Computational studies based on density functional theory (DFT) have used the reduced structure to generate models of a range of possible S-state intermediate structures.[9−17]

X-ray free electron laser (XFEL) sources generate ultra-intense, ultrashort laser pulses that provide the possibility of radiation damage-free X-ray structures. During XFEL experiments, the sample is destroyed due to the high intensity beam. Thus, serial femtosecond X-ray crystallography aims to overcome the radiation damage challenge by using XFEL pulses that induce diffraction on the femtosecond time scale

Received: August 22, 2017
Revised: September 14, 2017
Published: September 15, 2017

DOI: 10.1021/acs.jpcb.7b08371
J. Phys. Chem. B 2017, 121, 9382−9388

before the crystals are destroyed by the high intensity pulse field.[18] By exciting the crystals with a series of visible-light flashes at proper intervals immediately prior to X-ray irradiation, it becomes possible to explore the structures of the different S-states with such a technique. The S_1 structure of the OEC obtained by the short XFEL pulse[19] shows less radiation damage than the conventional X-ray structure.[20] However, it is unknown what radiation damage may still occur during the very short exposure time owing to the intensity of the X-ray pulse that can causes atomic ionization and subsequent ion−ion repulsion. The degree of damage is dependent on the beam characteristics, including energy, intensity, and pulse duration.[21] Thus, it is important to understand how the ultrashort time scale and ultra-intensity of pulses can distort the model of the OEC that is derived from the XFEL studies.

In the past few years, several crystal structures of the OEC have been solved by diffraction from an XFEL beam. However, the beam characteristics have greatly varied among the different measurements. For example, Shen and co-workers used a pulse duration of 10 fs,[19,22] while Yano and Yachandra group used pulses of 35 to 45 fs.[23] Fromme and co-workers used a longer pulse duration (50 fs).[24] Thus, in the calculations reported here, we will use Ehrenfest dynamics to study the correlation between the pulse duration and the radiation damage, which leads to suggestions for the appropriate pulse duration to obtain radiation damage-free structures.

We build upon an earlier study where we implemented ab initio molecular dynamics (AIMD) methods to study the correlation between the beam characteristics and radiation damage at the OEC, prepared in the resting S_1 state.[21] Here, we explore the sensitivity of the OEC to radiation damage along the S-state cycle as modulated by the geometrical and electronic structure of the OEC. We simulate the "diffraction-before-destruction" experiment using AIMD for different S-states keeping the beam characteristics fixed. We expose S_1, S_2, and S_3 model structures to an external field that mimics the XFEL beam and we determine the magnitude and direction of the structural changes induced by the beam due to displacement of each Mn, Ca, and μ-oxo in the various S-states. The aim is to determine whether changes in the positions of the ions induced by radiation damage could be detected by isomorphous Fourier differences of electron density maps of the different S-states. In addition, we compare radiation damage for the g = 2.0 and g = 4.1 spin isomers of the S_2 state as well as for the "open" and "closed" structural isomers of the S_3 state.

METHODS

TDDFT and Ehrenfest Dynamics. The calculations start from the DFT optimized structure in the localized orbital framework; the ground state wave function is obtained in the real space grid representation in OCTOPUS[25] with 0.18 Å grid spacing. Then, the time propagation method is used to evolve the ground state wave function in time with 0.002 fs time step in the presence of a Gaussian shaped laser field of 1.3×10^{15} W/cm^2. In addition, a mask wave function is applied on the borders of the simulation box to absorb the electronic flux and to properly model the ionization of the atoms. The temperature effect is considered through Fermi Dirac smearing. The ions are allowed to move in an Ehrenfest dynamics framework.

The model used for the AIMD includes the OEC, the amino acid ligands, and additional key residues (175 atoms) (Figure 1). The initial coordinates were obtained from the QM/MM

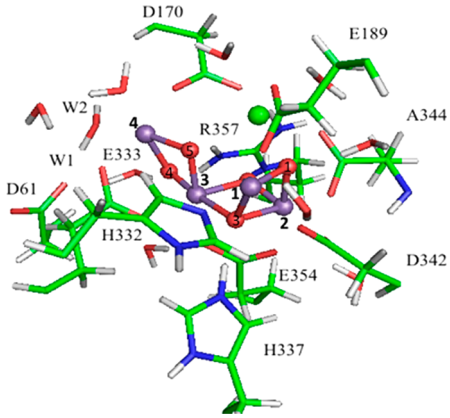

Figure 1. Model used for the AIMD calculations. The Mn are shown in magenta, Ca in green, and oxygens in red. R357 and E354 are from the CP43 subunit. All the other amino acids are from the D1 subunit. The Mn atoms are labeled with bold numbers. The oxygen labels are placed inside the red spheres.

structures reported in refs 9, 14, and 26. The initial structure for those models was taken from the 1.9 Å crystal structure (PDB code: 3ARC).[3] The reason that we used the 3ARC model and not the updated 3WU2 is that the differences are marginal and the system is minimized to the QM/MM local minima. The QM/MM model included all protein residues, cofactors, and crystallographic water molecules within 15 Å of any atom in the OEC. The peptide loops that were missing as a result of the cut were included in the models if they contained one or two protein residues. The rest of the chains were capped using ACE and NME groups (shown in square brackets). This resulted in the residue selection in Table 1.

Hydrogen atom placements were added using the AmberTools12 software package.[27] The residues having carboxylic side chains (ASP, GLU) were modeled as anions. Histidine protonation patterns were determined by inspection: His190 is protonated at N_δ to be a hydrogen-bond acceptor from D1-Tyr161, His332 is protonated at N_δ to leave N_ε as a ligand to Mn2, and His337 is protonated so that N_ε donates a hydrogen bond to O3. Hydrogens are added before minimization to fill the empty valences. Sodium counterions were added based on the electrostatic potential outside the protein to neutralize the system. There are 5 sodium ions added for S_0, 4 for S_1 and S_2 and 3 for S_3. Charges on the OEC atoms were assigned as previously reported.[28]

RESULTS AND DISCUSSION

The XFEL field induces atomic ionization and inelastic electron scattering through the sample.[29] The electron loss leads to accumulation of positive charge and an increase of repulsive potential energy, which in turn leads to increased kinetic energy for individual atoms in the cluster. The evolution of the kinetic energy through the pulse duration and its dependency on the beam intensity and energy has been studied extensively.[21] During the resulting Coulomb explosion, each ion experiences different forces due to their distinct surrounding environment and moves in the direction that minimizes the potential energy given the large electrostatic Coulomb repulsions. The initial temperature of the sample affects the thermal motion of the atoms. Thus, it is important to distinguish the atomic displacements induced by the XFEL field from the equilibrium thermal vibrational motion. However, because XFEL scattering

DOI: 10.1021/acs.jpcb.7b08371
J. Phys. Chem. B 2017, 121, 9382−9388

Table 1. Residue Selection

D1	CP43	D2
	[290]-291-[292]	
[57]-58-67-[68]	[305]-306-314-[315]	
[81]-82-91-[92]	[334]-335-337-[338]	[311]-312-321-[322]
[107]-108-112-[113]	[341]-342-[343]	[347]-348-352:[C-terminus]
[155]-156-192-[193]	[350]-351-358-[359]	
[289]-290-298-[299]	[398]-399-402-[403]	
[323]-324-344-[C-terminus]	[408]-409-413-[414]	

takes place in femtoseconds, measuring the induced structural changes experimentally is very difficult.

Ehrenfest dynamics and surface hopping[30] are techniques used to model the effect of nonadiabatic processes,[31,32] such as those induced by an external laser field, on classical molecular dynamics. In the surface hopping method, transitions between the adiabatic potential energy surfaces are implemented based on transition probabilities, while in Ehrenfest dynamics the systems propagate on the mean potential surface.[33] Ehrenfest dynamics has been used extensively to study nonadiabatic processes including the effect of an external laser field on molecules.[34−42] Here, we use *ab initio* Ehrenfest dynamics to study the effect of the XFEL beam on the system configuration of the OEC and surrounding residues.

Initially, we propagate the evolution of the electronic state and ionic coordinates of the S_1-state structure according to the Ehrenfest mean field forces, with no XFEL field applied to study the thermal motion, to compare the ionic motion due to the XFEL field to the equilibrium vibrational motion and to identify components responsible for the onset of radiation damage. It is known from model compounds that the internal Mn_4O_5Ca OEC cluster vibrational modes are in the low IR region $\upsilon < 700\ cm^{-1}$ (~50 fs).[43] Thus, the average atomic displacement due to room temperature motion of the 4 Mn centers in 50 fs is about 0.07 Å.

Our previous studies have shown that the radiation damage is independent of the beam intensity below a threshold of approximately 10^{18} W/cm^2.[21] Thus, because all of the OEC structures are solved experimentally using a beam intensity an order of magnitude lower than this threshold, we will fix the beam peak intensity at 1.3×10^{15} W/cm^2. In addition, due to the SASE (self-amplified spontaneous emission) nature of the XFEL beam, the generated shots have a bandwidth of ~40 eV and their intensity profile has significant variation.[44,45]

To consider the worst-case scenario, we have used a model beam field formed by a superposition of 5 Gaussians with different intensities spanning a frequency range of 40 eV similar to the SASE spectrum (Figure 2) where the intensity peaks near the beginning of the pulse. The beam has a median energy of 5 keV and pulse duration of 50 fs.

The energy of the XFEL beam is higher than the binding energy of most of the electrons in the system. Therefore, these electrons will be ejected from their orbitals and begin to move with different kinetic energies. Once they reach the boundaries of the simulation box they are absorbed due to the mask wave function placed on the boundaries (see Method section). Figure SI1 shows the electron loss through the 50 fs pulse. Due to the accumulated positive charges in the system, the ions start to move to reduce the potential energy.

Figure 3 shows the displacement of each Mn center of the OEC, relative to their initial coordinates as a function of time during the first 50 fs of dynamics under the influence of the

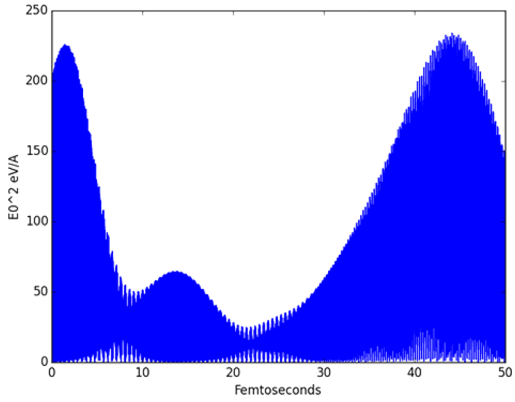

Figure 2. Intensity profile of the model X-ray pulse, formed by a superposition of 5 Gaussian pulses that span an energy range of 40 eV with a median energy of 5 keV.[45] The peak intensity is 1.3×10^{15} W/cm^2 and the pulse duration is 50 fs.

model pulse. In the dark-stable S_1 state, the formal charge has Mn1(III), Mn2(IV), Mn3(IV), Mn4(III), and each μ-oxo^{2-}. The "dangler" Mn4, which with two water ligands is less connected to the cluster, exhibits the largest deviation from the initial position (0.19 Å), then Mn1 (0.17 Å) and Mn2 (0.12 Å). The smallest deviation is observed for Mn3 (0.09 Å). The displacements of light oxo-bridges are much larger than those of heavier Mn centers, consistent with previous studies suggesting higher uncertainty about the positions of oxygen atoms that remain partially unresolved, even at 1.95 Å.[46,47] The average displacement of the μ-oxo ligands after 50 fs is 0.51 Å. These effects are intensity dependent as found previously.[21]

The net displacements, shown in Figure 3, result from both thermal vibrational motion and the influence of the XFEL field. To estimate the component due to the XFEL field, we subtracted the observed displacements after 50 fs in the absence of the field from the corresponding displacements of the structure exposed to the XFEL field. We find that the displacements due to the field are 0.14 and 0.10 Å for Mn4 and Mn2, respectively, and 0.20 and 0.10 Å for Mn1 and Mn3, respectively. Therefore, displacements due to the XFEL field during the 50 fs pulse are comparable in magnitude to displacements due to thermal fluctuations, although usually in a different direction. In addition, by integrating the electron density around the Mn centers, we found that the Mn ionization states do not change significantly from their initial states. The average translation induced by the XFEL field on the five μ-oxo oxygens is 0.31 Å during the first 50 fs, with a maximum displacement of 0.39 Å observed for O5, which alone among the oxygens changes position through the reaction. After 20 fs, the average displacement of the μ-oxo oxygens is 0.15 and 0.07 Å for the heavier Mn centers. Thus, in addition to the difficulty of resolving the electron density of the μ-oxo-

DOI: 10.1021/acs.jpcb.7b08371
J. Phys. Chem. B 2017, 121, 9382−9388

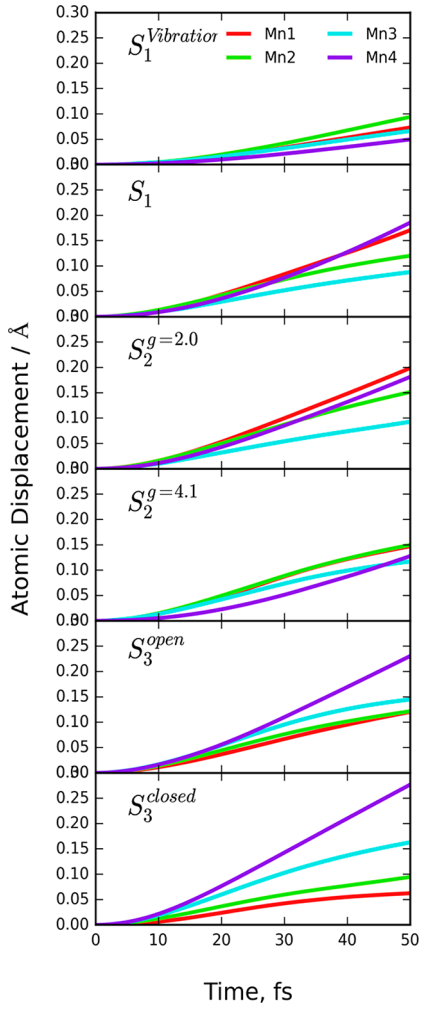

Figure 3. Displacements of the four Mn ions, in Å (*Y*-axis), as a function of time in fs (*X*-axis). Color key: Mn1 (red), Mn2 (green), Mn3 (cyan), and Mn4 (purple). Mn2 and Mn3 are IV in all states. Mn1 is III in S_1 and S_2 $g = 2$. Mn4 is III in S_1 and S_2 $g = 4.1$. In the S_3 structures all Mn are in the IV state.

bridges because of the density of the neighboring Mn ions,[46] radiation damage also decreases the accuracy of the experimental oxygen positions.

The $S_1 \rightarrow S_2$ transition is due to oxidation of either Mn4 ($g = 2$ structure) or Mn1 ($g = 4.1$ structure), leading to formation of two states of similar energy.[48,49] The $g = 2$ isomer has a total spin of $S = 1/2$ and a shorter Mn4−O5 bond, while the $g = 4.1$ has a spin of $S = 5/2$ and a shorter Mn1−O5 bond. Both S_2 isomers have the same number of atoms as the S_1 state because there is no deprotonation during the $S_1 \rightarrow S_2$ transition. Therefore, there is an extra positive charge accumulated on the cluster. The S_2 structure is thus expected to be more susceptible to Coulomb explosion than S_1. In the $g = 2$ structure, due to oxidation of the dangler Mn4 to Mn(IV), the translation pattern of the Mn ions is similar to that of the S_1 state (with maximum displacements for Mn1 and Mn4 and minimum for Mn3). However, the overall displacements are on average larger in the S_2 state due to the larger repulsive potential.

The S_2 $g = 4.1$ isomer, with Mn1 oxidized to Mn(IV) during the $S_1 \rightarrow S_2$ transition, exhibits a different pattern of displacements induced by the XFEL field. The Mn1 center is part of the OEC cuboidal structure and its oxidation induces more significant displacements for Mn1 and Mn2 than for Mn3 and Mn4. Thus, although the two S_2 isomers have the same number of atoms and the same charge, the different electronic structure leads them to respond differently to the XFEL field.

We observe a clear correlation between the ligand environment/oxidation state of Mn ions and their resulting displacements. The key difference is that when Mn4 is oxidized to Mn(IV) and attains a complete 6-coordinate ligation shell in the $g = 2$ S_2-state isomer, it exhibits a large deviation from the S_1-state coordinates. In the $g = 4.1$ S_2-state isomer, however, Mn4 exhibits less significant displacement since it has an incomplete 5-coordinate ligation shell and is relatively separated from the Mn_3O_4Ca cube. The onset of the Coulomb explosion increases the separation between positively charged ions and centers with higher charges, such as Mn(IV), experience more significant displacements than the less charged Mn(III) centers. In addition, the Mn-ligand distances are shorter in the higher oxidation states. Thus, the higher oxidation-state Mn ions are subject to greater radiation damage in the comparison of the two S_2-state isomers.

The $S_2 \rightarrow S_3$ transition involves oxidation of the last Mn(III) in the cluster and deprotonation to the lumen to balance the accumulated positive charges on the OEC.[50] The resulting proton-coupled electron-transfer (PCET) causes larger structural changes when compared to those of the $S_1 \rightarrow S_2$ transition, consistent with EXAFS measurements,[11,51−53] and is thought to involve binding of a water molecule to the OEC core, forming an additional oxo-bridge.[16,54,55] Current models for the S_3 state include "open" and "closed" structures of the Mn_4O_5Ca cubane.[12−17] Some studies suggest that both structures may play a role in different stages of the catalytic cycle.[14] We find that the radiation-damage pattern is similar for the two structures. However, in the "open" structure, Mn4 and Mn1 exhibit smaller displacements than in the "closed" form, while Mn2 and Mn3 exhibit more significant displacements in the "open" structure.

In general, there is no clear correlation between specific Mn displacement in the different states due to the radiation damage. However, the overall displacement increases in the advanced S-states due to the accumulation of positive charges, which increases the potential energy of the system, and we expect this to be found in XFEL studies of different metalloproteins.

For each structure, the atomic displacements induced by the XFEL field correspond to the displacements that reduce the ion−ion repulsion. As shown in Table 2, the angles of divergence are different for the different S-states with no simple correlation between the directions of motion for the different structures. Thus, caution must be taken when analyzing Fourier difference maps between two states since XFEL induced displacements will not be canceled. For example, the latest study by Young et al. suggests that Mn−Mn distances are shortened and W3 and W4 are displaced toward E189 and D170, respectively, in the S_3 structure.[23] However, our simulations suggest that the Mn−Mn and W3-to-D179 distances would increase due to the influence of the pulse, although the W4 to E189 distance is reduced by 0.1 Å. Thus, radiation-induced changes may lead to an underestimation of some displacements and overestimation of others, particularly when using typical pulses of 35−45 fs.

The location of the two oxygens that form O_2 during the $S_4 \rightarrow S_0$ transition remains a subject of great interest. Formation of the O═O bond requires a reduction of the distance between

DOI: 10.1021/acs.jpcb.7b08371
J. Phys. Chem. B 2017, 121, 9382−9388

Table 2. Scattering Angles of the Mn Ions Due to Coulomb Explosion[a]

	S_1	S_2	S_3^{open}
∠O5-Mn4-$Mn4_f$	142	125	92
∠O4-Mn4-$Mn4_f$	130	82	170
∠W2-Mn4-$Mn4_f$	53	102	8
∠O3-Mn1-$Mn1_f$	120	104	117
∠O1-Mn1-$Mn1_f$	80	81	147
∠O5-Mn1-$Mn1_f$	158	39	132
∠O4-Mn3-$Mn3_f$	69	139	142
∠O2-Mn3-$Mn3_f$	119	80	68
∠O3-Mn3-$Mn3_f$	114	39	137
∠O3-Mn2-$Mn2_f$	137	75	84
∠O2-Mn2-$Mn2_f$	76	103	168
∠O1-Mn2-$Mn2_f$	136	144	84

[a]All the angles are in degrees. The subscript f indicates the final position after 50 fs. The correlation coefficient R^2 between the scattering angles of the ions in the S_1 and S_2 is of 0.08, S_2 and S_3 have R^2 of 0.03, and R^2 0.007 of for S_1 and S_3.

the oxygens forming the O_2 molecule. Our calculations suggest that the distance between O5 and the additional oxygen inserted during the S_2-to-S_3 transition can decrease from 2.8 to 2.6 Å in about 50 fs, simply due to the influence of the XFEL field. Thus, the recommended pulse duration for studies of the O═O bond formation should be shorter than 15 fs for typical intensities, so that the change in the reactive oxygen-to-oxygen distance will not exceed 0.1 Å.

In summary, the simulations suggest that the displacement of ions, due to the influence of the XFEL field, is less than 0.05 Å when the pulse duration is less than 10 fs for any S-state. After 15 fs, the oxo-bridges exhibit displacements larger than 0.1 Å, although displacements of Mn ions remain smaller than 0.05 Å. However, significant displacements above thermal fluctuations may be observed when the pulse duration exceeds 40 fs. Table 3 shows the beam characteristics for the different XFEL structures obtained for photosystem II. The structures by Suga et al.[19,22] are obtained with a beam of pulse duration equal to or shorter than 10 fs and considered radiation damage free based on our simulations.

CONCLUSIONS

We have shown that structural changes induced by the XFEL field are dependent on the electronic state and molecular conformation of the atoms in a cluster. For the Mn_4O_5Ca OEC cluster, the atomic displacements induced by the XFEL field are smaller in the less oxidized S_1 structure. However, oxidation of the cluster to the S_2 state accumulates a positive charge, which increases the ionic repulsion and, therefore, the resulting ionic displacements. The simulations suggest that for the analyzed beam intensities (i.e., peak intensity of 1.3×10^{15} W/cm^2), structures exposed to pulses of duration of less than 15 fs may be considered free of radiation damage. Although the calculated ionic displacement is significantly below the resolution of current XFEL crystal structure models of the OEC, these changes maybe significant when comparing isomorphous Fourier differences of electron density maps for different S-states. In particular, XFEL induced motions may suggest shorter oxygen-to-oxygen distances which should not be misinterpreted as the actual changes in interatomic distances required for O═O bond formation.

ASSOCIATED CONTENT

Supporting Information

The Supporting Information is available free of charge on the ACS Publications website at DOI: 10.1021/acs.jpcb.7b08371.

Figures that show the evolution of the electronic charges and the energies through 50 fs; input structures used in the simulations and sample input file of the Ehrenfest dynamics (PDF)

AUTHOR INFORMATION

Corresponding Author

*E-mail: muhamed.amin@cfel.de. Tel:+49(0)4089986345.

ORCID

Muhamed Amin: 0000-0002-3146-150X

Victor S. Batista: 0000-0002-3262-1237

Gary W. Brudvig: 0000-0002-7040-1892

Notes

The authors declare no competing financial interest.

ACKNOWLEDGMENTS

We would like to thank Dr. Angel Rubio and his group for the useful discussion. We acknowledge support from European Research Council through the Consolidator Grant COMOTION (ERC-Küpper-614507), the Division of Chemical Sciences, Geosciences, and Biosciences, Office of Basic Energy Sciences, U.S. Department of Energy (DE-SC0001423 and DE-FG02-05ER15646) and computational resources from NERSC and Bibliotheca Alexandria.

REFERENCES

(1) Joliot, P.; Kok, B. Oxygen evolution in photosynthesis. In *Bioenergetics of Photosynthesis*, Govindjee, Ed.; Academic Press: New York, 1975; pp 387−412.

(2) Kok, B.; Forbush, B.; McGloin, M. Cooperation of charges in photosynthetic O_2 evolution-I. A linear four step mechanism. *Photochem. Photobiol.* **1970**, *11* (6), 457−75.

Table 3. Beam Characteristics of the Different XFEL Structures of Photosystem II[a]

PDB ID	illumination	resolution Å	pulse duration (femtoseconds)	beam energy (keV)	beam intensity
5GTH	S_1	2.50	2−10	7	8.7×10^{16} W/cm^2
5GTI	S_3	2.50	2−10	7	8.7×10^{16} W/cm^2
4UB6	S_1	1.95	10 or shorter	10	4.2×10^{16} W/cm^2
5KAF	S_1	3.00	35−45	NA	3.0×10^{15} W/cm^2
5TIS	S_3	2.25	35−45	NA	3.0×10^{15} W/cm^2
4RVY	S_3	5.50	50	6	NA

[a]NA indicates that the data are not available. Based on our simulations, only the 5GTH, 5GTI, and 4UB6 structures are considered radiation damage free.

DOI: 10.1021/acs.jpcb.7b08371
J. Phys. Chem. B 2017, 121, 9382−9388

(3) Umena, Y.; Kawakami, K.; Shen, J.-R.; Kamiya, N. Crystal structure of oxygen-evolving photosystem II at 1.9 A resolution. *Nature* **2011**, *473* (7345), 55−60.
(4) Brudvig, G. W. Water oxidation chemistry of photosystem II. *Philos. Trans. R. Soc., B* **2008**, *363* (1494), 1211−8 discussion 1218−9..
(5) Brudvig, G. W.; Beck, W. F.; de Paula, J. C. Mechanism of photosynthetic water oxidation. *Annu. Rev. Biophys. Biophys. Chem.* **1989**, *18*, 25−46.
(6) Schilstra, M. J.; Rappaport, F.; Nugent, J. H.; Barnett, C. J.; Klug, D. R. Proton/hydrogen transfer affects the S-state-dependent microsecond phases of P680+ reduction during water splitting. *Biochemistry* **1998**, *37* (11), 3974−81.
(7) Luber, S.; Rivalta, I.; Umena, Y.; Kawakami, K.; Shen, J. R.; Kamiya, N.; Brudvig, G. W.; Batista, V. S. S1-state model of the O_2-evolving complex of photosystem II. *Biochemistry* **2011**, *50* (29), 6308−11.
(8) Vogt, L.; Ertem, M. Z.; Pal, R.; Brudvig, G. W.; Batista, V. S. Computational insights on crystal structures of the oxygen-evolving complex of photosystem II with either Ca(2+) or Ca(2+) substituted by Sr(2+). *Biochemistry* **2015**, *54* (3), 820−5.
(9) Pal, R.; Negre, C. F.; Vogt, L.; Pokhrel, R.; Ertem, M. Z.; Brudvig, G. W.; Batista, V. S. S_0-state model of the oxygen-evolving complex of Photosystem II. *Biochemistry* **2013**, *52* (44), 7703−6.
(10) Sproviero, E. M.; Gascon, J. A.; McEvoy, J. P.; Brudvig, G. W.; Batista, V. S. Computational insights into the oxygen-evolving complex of Photosystem II. *Photosynth. Res.* **2008**, *97*, 91.
(11) Sproviero, E. M.; Gascon, J. A.; McEvoy, J. P.; Brudvig, G. W.; Batista, V. S. A model of the oxygen-evolving center of photosystem II predicted by structural refinement based on EXAFS simulations. *J. Am. Chem. Soc.* **2008**, *130* (21), 6728−30.
(12) Ugur, I.; Rutherford, A. W.; Kaila, V. R. Redox-coupled substrate water reorganization in the active site of Photosystem II-The role of calcium in substrate water delivery. *Biochim. Biophys. Acta, Bioenerg.* **2016**, *1857* (6), 740−748.
(13) Retegan, M.; Krewald, V.; Mamedov, F.; Neese, F.; Lubitz, W.; Cox, N.; Pantazis, D. A. A five-coordinate Mn (iv) intermediate in biological water oxidation: spectroscopic signature and a pivot mechanism for water binding. *Chemical Science* **2016**, *7*, 72.
(14) Askerka, M.; Wang, J.; Vinyard, D. J.; Brudvig, G. W.; Batista, V. S. S_3 state of the O_2-evolving complex of Photosystem II: insights from QM/MM, EXAFS, and femtosecond X-ray diffraction. *Biochemistry* **2016**, *55* (7), 981−4.
(15) Askerka, M.; Vinyard, D. J.; Brudvig, G. W.; Batista, V. S. NH_3 Binding to the S_2 state of the O_2-evolving complex of Photosystem II: analogue to H2O binding during the S_2 –> S_3 transition. *Biochemistry* **2015**, *54* (38), 5783−6.
(16) Li, X. C.; Siegbahn, P. E. M. Alternative mechanisms for O_2 release and O-O bond formation in the oxygen evolving complex of photosystem II. *Phys. Chem. Chem. Phys.* **2015**, *17* (18), 12168−12174.
(17) Capone, M.; Narzi, D.; Bovi, D.; Guidoni, L. Mechanism of Water Delivery to the Active Site of Photosystem II along the S(2) to S(3) Transition. *J. Phys. Chem. Lett.* **2016**, *7* (3), 592−6.
(18) Chapman, H. N.; Fromme, P.; Barty, A.; White, T. A.; Kirian, R. A.; Aquila, A.; Hunter, M. S.; Schulz, J.; DePonte, D. P.; Weierstall, U.; et al. Femtosecond X-ray protein nanocrystallography. *Nature* **2011**, *470* (7332), 73−7.
(19) Suga, M.; Akita, F.; Hirata, K.; Ueno, G.; Murakami, H.; Nakajima, Y.; Shimizu, T.; Yamashita, K.; Yamamoto, M.; Ago, H.; et al. Native structure of photosystem II at 1.95 A resolution viewed by femtosecond X-ray pulses. *Nature* **2014**, *517* (7532), 99−103.
(20) Davis, K. M.; Pushkar, Y. N. Structure of the oxygen evolving complex of Photosystem II at room temperature. *J. Phys. Chem. B* **2015**, *119* (8), 3492−8.
(21) Amin, M.; Badawi, A.; Obayya, S. S. Radiation damage in XFEL: case study from the oxygen-evolving complex of Photosystem II. *Sci. Rep.* **2016**, *6*, 36492.
(22) Suga, M.; Akita, F.; Sugahara, M.; Kubo, M.; Nakajima, Y.; Nakane, T.; Yamashita, K.; Umena, Y.; Nakabayashi, M.; Yamane, T.; et al. Light-induced structural changes and the site of O=O bond formation in PSII caught by XFEL. *Nature* **2017**, *543* (7643), 131−135.
(23) Young, I. D.; Ibrahim, M.; Chatterjee, R.; Gul, S.; Fuller, F. D.; Koroidov, S.; Brewster, A. S.; Tran, R.; Alonso-Mori, R.; Kroll, T.; et al. Structure of photosystem II and substrate binding at room temperature. *Nature* **2016**, *540* (7633), 453−457.
(24) Kupitz, C.; Basu, S.; Grotjohann, I.; Fromme, R.; Zatsepin, N. A.; Rendek, K. N.; Hunter, M. S.; Shoeman, R. L.; White, T. A.; Wang, D.; et al. Serial time-resolved crystallography of photosystem II using a femtosecond X-ray laser. *Nature* **2014**, *513* (7517), 261−5.
(25) Andrade, X.; Strubbe, D.; De Giovannini, U.; Larsen, A. H.; Oliveira, M. J.; Alberdi-Rodriguez, J.; Varas, A.; Theophilou, I.; Helbig, N.; Verstraete, M. J.; et al. Real-space grids and the Octopus code as tools for the development of new simulation approaches for electronic systems. *Phys. Chem. Chem. Phys.* **2015**, *17* (47), 31371−96.
(26) Askerka, M.; Wang, J.; Brudvig, G. W.; Batista, V. S. Structural changes in the oxygen-evolving complex of photosystem II induced by the S_1 to S_2 transition: A combined XRD and QM/MM study. *Biochemistry* **2014**, *53* (44), 6860−2.
(27) Case, D. A.; Cheatham, T. E., III; Simmerling, C. L.; Wang, J.; Duke, R. E.; Luo, R.; Walker, R. C.; Zhang, W.; Merz, K. M.; Roberts, B.; Hayik, S.; Roitberg, A.; Seabra, G.; Swails, J.; Goetz, A. W.; Kolossváry, I.; Wong, K. F.; Paesani, F.; Vanicek, J.; Wolf, R. M.; Liu, J.; Wu, X.; Brozell, S. R.; Steinbrecher, T.; Gohlke, H.; Cai, Q.; Ye, X.; Wang, J.; Hsieh, M.-J.; Cui, G.; Roe, D. R.; Mathews, D. H.; Seetin, M. G.; Salomon-Ferrer, R.; Sagui, C.; Babin, V.; Luchko, T.; Gusarov, S.; Kovalenko, A.; Kollman, P. A. *AMBER 12*; University of California, San Francisco, 2012.
(28) Sproviero, E. M.; Gascon, J. A.; McEvoy, J. P.; Brudvig, G. W.; Batista, V. S. Quantum mechanics/molecular mechanics study of the catalytic cycle of water splitting in photosystem II. *J. Am. Chem. Soc.* **2008**, *130* (11), 3428−42.
(29) Neutze, R.; Wouts, R.; van der Spoel, D.; Weckert, E.; Hajdu, J. Potential for biomolecular imaging with femtosecond X-ray pulses. *Nature* **2000**, *406* (6797), 752−7.
(30) Parandekar, P. V.; Tully, J. C. Mixed quantum-classical equilibrium. *J. Chem. Phys.* **2005**, *122* (9), 094102.
(31) Batista, V. S.; Coker, D. F. Nonadiabatic molecular dynamics simulation of photodissociation and geminate recombination of I2 liquid xenon. *J. Chem. Phys.* **1996**, *105* (10), 4033−4054.
(32) Rego, L. G.; Batista, V. S. Quantum dynamics simulations of interfacial electron transfer in sensitized TiO_2 semiconductors. *J. Am. Chem. Soc.* **2003**, *125* (26), 7989−97.
(33) Zimmermann, T.; Vanicek, J. Efficient on-the-fly ab initio semiclassical method for computing time-resolved nonadiabatic electronic spectra with surface hopping or Ehrenfest dynamics. *J. Chem. Phys.* **2014**, *141* (13), 134102.
(34) Bastida, A.; Cruz, C.; Zuniga, J.; Requena, A.; Miguel, B. The Ehrenfest method with quantum corrections to simulate the relaxation of molecules in solution: equilibrium and dynamics. *J. Chem. Phys.* **2007**, *126* (1), 014503.
(35) Isborn, C. M.; Li, X.; Tully, J. C. Time-dependent density functional theory Ehrenfest dynamics: collisions between atomic oxygen and graphite clusters. *J. Chem. Phys.* **2007**, *126* (13), 134307.
(36) Li, X.; Tully, J. C.; Schlegel, H. B.; Frisch, M. J. Ab initio Ehrenfest dynamics. *J. Chem. Phys.* **2005**, *123* (8), 084106.
(37) Liang, W.; Isborn, C. M.; Li, X. Laser-controlled dissociation of C2H2(2+): Ehrenfest dynamics using time-dependent density functional theory. *J. Phys. Chem. A* **2009**, *113* (15), 3463−9.
(38) Liang, W.; Isborn, C. M.; Lindsay, A.; Li, X.; Smith, S. M.; Levis, R. J. Time-dependent density functional theory calculations of Ehrenfest dynamics of laser controlled dissociation of NO+: pulse length and sequential multiple single-photon processes. *J. Phys. Chem. A* **2010**, *114* (21), 6201−6.
(39) Miyamoto, Y.; Tateyama, Y.; Oyama, N.; Ohno, T. Conservation of the pure adiabatic state in Ehrenfest dynamics of the photoisomerization of molecules. *Sci. Rep.* **2016**, *5*, 18220.

DOI: 10.1021/acs.jpcb.7b08371
J. Phys. Chem. B 2017, 121, 9382−9388

(40) Saita, K.; Shalashilin, D. V. On-the-fly ab initio molecular dynamics with multiconfigurational Ehrenfest method. *J. Chem. Phys.* **2012**, *137* (22), 22A506.
(41) Seki, Y.; Takayanagi, T.; Shiga, M. Photoexcited Ag ejection from a low-temperature He cluster: a simulation study by nonadiabatic Ehrenfest ring-polymer molecular dynamics. *Phys. Chem. Chem. Phys.* **2017**, *19* (21), 13798−13806.
(42) Wang, F.; Yam, C. Y.; Hu, L.; Chen, G. Time-dependent density functional theory based Ehrenfest dynamics. *J. Chem. Phys.* **2011**, *135* (4), 044126.
(43) Chu, H. A.; Hillier, W.; Law, N. A.; Babcock, G. T. Vibrational spectroscopy of the oxygen-evolving complex and of manganese model compounds. *Biochim. Biophys. Acta, Bioenerg.* **2001**, *1503* (1−2), 69−82.
(44) Ding, Y.; Brachmann, A.; Decker, F. J.; Dowell, D.; Emma, P.; Frisch, J.; Gilevich, S.; Hays, G.; Hering, P.; Huang, Z.; et al. Measurements and simulations of ultralow emittance and ultrashort electron beams in the linac coherent light source. *Phys. Rev. Lett.* **2009**, *102* (25), 254801.
(45) Makita, M.; Karvinen, P.; Zhu, D.; Juranic, P. N.; Grünert, J.; Cartier, S.; Jungmann-Smith, J. H.; Lemke, H. T.; Mozzanica, A.; Nelson, S.; Patthey, L.; Sikorski, M.; Song, S.; Feng, Y.; David, C. High-resolution single-shot spectral monitoring of hard x-ray free-electron laser radiation. *Optica* **2015**, *2* (10), 912−916.
(46) Askerka, M.; Vinyard, D. J.; Wang, J.; Brudvig, G. W.; Batista, V. S. Analysis of the radiation-damage-free X-ray structure of photosystem II in light of EXAFS and QM/MM data. *Biochemistry* **2015**, *54* (9), 1713−6.
(47) Askerka, M.; Brudvig, G. W.; Batista, V. S. The O_2-evolving complex of Photosystem II: recent insights from quantum mechanics/molecular mechanics (QM/MM), extended X-ray absorption fine structure (EXAFS), and femtosecond X-ray crystallography data. *Acc. Chem. Res.* **2017**, *50* (1), 41−48.
(48) Pantazis, D. A.; Ames, W.; Cox, N.; Lubitz, W.; Neese, F. Two interconvertible structures that explain the spectroscopic properties of the oxygen-evolving complex of photosystem II in the S_2 state. *Angew. Chem., Int. Ed.* **2012**, *51* (39), 9935−40.
(49) Amin, M.; Pokhrel, R.; Brudvig, G. W.; Badawi, A.; Obayya, S. S. Effect of chloride depletion on the magnetic properties and the redox leveling of the oxygen-evolving complex in Photosystem II. *J. Phys. Chem. B* **2016**, *120* (18), 4243−8.
(50) Amin, M.; Vogt, L.; Szejgis, W.; Vassiliev, S.; Brudvig, G. W.; Bruce, D.; Gunner, M. R. Proton-coupled electron transfer during the S-state transitions of the oxygen-evolving complex of Photosystem II. *J. Phys. Chem. B* **2015**, *119* (24), 7366−77.
(51) Hasegawa, K.; Ono, T.; Inoue, Y.; Kusunoki, M. How to evaluate the structure of a tetranuclear Mn cluster from magnetic and EXAFS data: Case of the S_2-state Mn-cluster in photosystem II. *Bull. Chem. Soc. Jpn.* **1999**, *72* (5), 1013−1023.
(52) Riggs-Gelasco, P. J.; Mei, R.; Yocum, C. F.; Penner-Hahn, J. E. Reduced derivatives of the Mn cluster in the oxygen-evolving complex of photosystem II: An EXAFS study. *J. Am. Chem. Soc.* **1996**, *118* (10), 2387−2399.
(53) Yano, J.; Pushkar, Y.; Glatzel, P.; Lewis, A.; Sauer, K.; Messinger, J.; Bergmann, U.; Yachandra, V. High-resolution Mn EXAFS of the oxygen-evolving complex in photosystem II: Structural implications for the Mn4Ca cluster. *J. Am. Chem. Soc.* **2005**, *127* (43), 14974−14975.
(54) Noguchi, T. FTIR detection of water reactions in the oxygen-evolving centre of photosystem II. *Philos. Trans. R. Soc., B* **2008**, *363* (1494), 1189−1194.
(55) Dau, H.; Liebisch, P.; Haumann, M. The manganese complex of oxygenic photosynthesis: Conversion of five-coordinated Mn(III) to six-coordinated Mn(IV) in the S_2-S_3 transition is implied by XANES simulations. *Phys. Scr.* **2005**, *T115*, 844−846.

DOI: 10.1021/acs.jpcb.7b08371
J. Phys. Chem. B 2017, 121, 9382−9388